# IrisTac: A Vision-based Tactile Sensor with Chromatic and Modeled Illumination

1st Xin Liu
*Department of Mechanical and Energy Engineering*
*Southern University of Science and Technology (SUSTech)*
Shenzhen, China
12131091@mail.sustech.edu.cn

2nd Lijie Sheng
*Department of Mechanical and Energy Engineering*
*Southern University of Science and Technology (SUSTech)*
Shenzhen, China
12011127@mail.sustech.edu.cn

3rd Yige Wu
*Department of Mechanical and Energy Engineering*
*Southern University of Science and Technology (SUSTech)*
Shenzhen, China
12232329@mail.sustech.edu.cn

4th Isabel Y.N Guan
*School of Software and Microelectronics*
*Peking University*
Beijing, China
yani_guan@outlook.com

5th Zheng Zhu
*Department of Mechanical and Energy Engineering*
*Southern University of Science and Technology (SUSTech)*
Shenzhen, China
zhuz@sustech.edu.cn

6th Zhenzhong Jia*
*Department of Mechanical and Energy Engineering*
*Southern University of Science and Technology (SUSTech)*
Shenzhen, China
jiazz@sustech.edu.cn
*Corresponding author

***Abstract*—This paper demonstrates a new tactile sensor design, IrisTac, specifically designed to simulate different lighting environments. We refer to most of the previous literature on optimizing optical design for tactile sensors, resulting in a combination of a phantom LED ring and an optical lens. Thanks to our light source design, we can simulate various lighting conditions and achieve brightness supplementation by adjusting each independent LED's color ratios and light emission levels. With the help of an optical lens, we improve the path of the incident light, ensuring almost all the light emitted by LED can be uniformly irradiated on the imaging surface. During the development of the lens, we create an environment specifically for light path simulation, which can aid us and other researchers in achieving rapid design. All these optimizations are integrated into a compact sensor that is easy to manufacture, assemble, use, and maintain. Our work provides not only a solution for design iterations of tactile sensors but also a valuable tool for others who wish to continue exploring the field of optical optimization in tactile sensors.**

***Keywords*—IrisTac, tactile sensor design, optical design, phantom LED, optical lens design**

## I. Introduction

As an essential part of robotic manipulation tasks, sensory technology progressively bifurcates into two distinct pathways—visual and tactile. Amid these two distinct domains, tactile sensors hold a crucial position as an integral perceptual technology. With ongoing technological advancements, tactile sensors have progressively gained the ability to determine the orientation and shape of an object, perceive surface textures, and quantify applied forces and moments on a contact surface. With this information, robots can effectively perform operations such as grasping, manipulation, and assembly.

Based on the different principles of simulating tactile mechanisms, tactile sensors can be classified into various types, such as resistive sensors, capacitive sensors, and fiber sensors. Among these sensors, vision-based tactile sensors (VBTS) overcome the obstacle of achieving high resolution within confined spaces. The tactile information extracted from tactile images is accomplished through image processing techniques. Since images provide continuous tactile information, it is easy to significantly improve the performance of the tactile sensor by enhancing the resolution of the camera and refining the extraction methodology.

Conventional VBTSs typically comprise three systems: an illumination system, a camera system, and a contact sensing system. When the sensor contacts the object measured, the contact sensing system undergoes deformation along the contact surface. Simultaneously, the illumination system emits light that reflects off the deformed surface and is captured by the camera system. Algorithms then analyze the images taken before and after the deformation of the contact sensing system to determine the changing distribution of brightness and darkness within the image. This information can be further

Shenzhen Key Laboratory of Biomimetic Robotics and Intelligent Systems, Department of Mechanical and Energy Engineering, Southern University of Science and Technology (SUSTech), Shenzhen, 518055, China. Guangdong Provincial Key Laboratory of Human-Augmentation and Rehabilitation Robotics in Universities, SUSTech, Shenzhen, 518055, China.
*Corresponding author: jiazz@sustech.edu.cn

processed to extract tactile data.

The core algorithm used for image processing is Photometric Stereo Algorithm, which places strict demands on the uniformity of internal illumination. These stringent requirements add complexity to the design of the optical system and its corresponding electromechanical system. Recently, many scholars have regarded the enhancement of the light system as a pivotal breakthrough point in the VBTS field. For example, Taylor et al. [1] used illuminations shaping lens to improve the concentration of light, Wang et al. [2]installed a diffuser and gray filter front of the light source, and Dong et al. [3] used tricolor light in GelSight to produce more image information. Although all of these advancements in sensor technology are significant, we believe that there is still value in exploring the optimization of illumination systems.

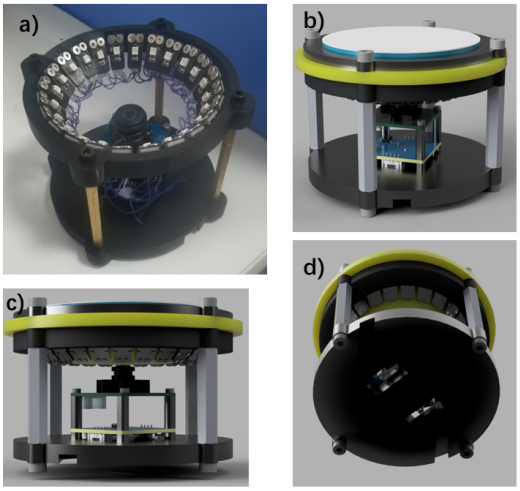


Fig. 1. (a) Finished product of IrisTac. (b) Vertical view of IrisTac. (c) Front view of IrisTac. (d) Bottom view of IrisTac.

We advocate to improve the performance of the sensor by optimizing the optical design. The main contributions of this paper are:

- We innovatively use 24 controllable phantom LEDs as the light source and controll the RGB intensity of each LED to change the illumination conditions. This approach enables us to effectively meet the photometric stereo algorithm's requirements. Additionally, we incorporate a lens into the design to manipulate the light paths and achieve uniform illumination across the sensor's surface. Guided by these principles, we have developed the IrisTac sensor.
- IrisTac offers several advantages, including minimal components, streamlined manufacturing processes, and a highly integrated circuit design. Using the IrisTac template, the development of new tactile sensors can be expedited effectively.
- We build a system to realize the simulation of the light path, which helps us design a lens. We also design a reasonable external interface to support the secondary development for other researchers.

The rest of the paper is organized as follows: In Part II, we will present a paper review on vision-based tactile sensors and photometric stereo algorithms, specifically focusing on optical design. We will discuss the motivations behind the light source design of IrisTac in Part III. Part IV will outline the principles of light path simulation and provide specific details regarding lens design. In Part V, we will present the sensor design and conduct experiments to validate our theories. Finally, the paper concludes with a summary and conclusions in Part VII.

## II. Related Work

### A. Vision-based tactile sensors

Based on hardware structure, vision-based tactile sensors can be classified by the manufacturing process of contact gel, reflective coating type, optical path design, camera type, and so on. Due to this paper's focus on optical design, we will analyze the differences in light path optimization.

LEDs are often chosen as light sources for compact integrated systems because of their small size and high brightness. The earliest batch of tactile sensors led by GelSight [3] always used a single LED as an independent light source. However, Donlon et al. [4] suggested that rows of LEDs provide more uniform illumination in a given dimension, so a group of VBTSs chose to use multiple LEDs as the light source. Even after implementing the RGB tricolor light scheme in GelSlim3.0 [1], they opted to continue using a group of lights instead of a single LED as a monochromatic light source.

Unlike diversity in number and combination, the brightness of LEDs is usually constant; only a few papers mentioned the control of LED brightness; Lambet et al. [5] attempted to use MCU integrated in PCB to control the brightness of all the LEDs.

As for the color types of LEDs, VBTSs are classified into two types: RGB tri-color light and pure white light. GelSight [3] designed a trichromatic LED illumination system, strengthening the linear relationship between the direction of contact surface normal and the color change of tactile image by providing richer color variations. Additionally, tricolor light is often seen as a "trading space for time" approach. We can separate three independent light maps from one three-color illumination image instead of three separate shots. GelSlim 3.0 [1] used this approach to build a lookup table of the brightness values on three channels and surface normal directions. Apart from this, there are many other novel color combinations; Hogan et al. [6] placed red, green, blue, and white LEDs on each side of a rectangular sensor. Conversely, some VBTSs can be implemented by monochromatic light, Lin et al. [7] achieved surface height reconstruction by using single white light based on the difference in darkness shown in the captured image.

In addition tothe different numbers and types of LEDs, researchers have begun to seek innovation on the light path. Based on the direction of incidence light, VBTSs can be broadly divided into two types—vertical illumination and side illumination. Vertical illumination is more effective than side illumination because we can avoid the generation of shadows

TABLE I
COMPARISON BETWEEN DIFFERENT VISION-BASED TACTILE SENSORS AND OUR SENSOR AT THE OPTICAL OPTIMIZATION LEVEL

| *Senser Type* | **Characteristics of various vision-based tactile sensors** | | | |
|---|---|---|---|---|
| | ***Use multi-color light*** | ***Optimizing light with optical lenses*** | ***the intensity of the light source is adjustable*** | ***Use LED Set*** |
| IrisTac(***Our sensor***) | Yes(all colors) | Yes | Yes | Yes |
| GelSight | Yes(RGB three colors) | No | No | Yes |
| GelSight Wedge | Yes(RGB three colors) | Yes | No | Yes |
| GelSlim | No | Yes | No | Yes |
| GelSlim3.0 | Yes(RGB three colors) | Yes | No | Yes |
| DIGIT | Yes(RGB three colors) | No | Yes | No |
| DTact | No | No | No | Yes |
| STS | Yes(RGBW four colors) | No | No | Yes |
| TS(H.Jiang st al.) | No | No | No | No |

and the brightness attenuation that occurs as the irradiation distance becomes longer. For example, Jiang et al [8] placed four white light-emitting diodes above the camera and facing the same direction. Compared to the previous method, side illumination allows for the center area of the contact surface to be well-illuminated, but the edge area lacks sufficient brightness. To combine the two advantages of space saving and uniform light illumination, some researchers used optical lenses to realize changes to the light path. For example, GelSlim [4] used parabolic mirrors to focus the light and turn the point light source into parallel light, Zhang et al. [9] used four mirrors to enable a monocular camera to realize the binocular vision, GelSlim 3.0 [1] utilized a hexagonal prism to distribute the illumination over the entire surface of the sensor uniformly. Wang et al. [2] used diffuser and gray filter front LED. The diffuser smoothly disperses the light for a more uniform overall illumination, while the gray filter absorbs the light to reduce internal reflections.

Our optical design includes both light source design and lens design. Based on the above papers we use a LED ring with adjustable brightness and color ratios. Besides, we simultaneously designed optical lenses to meet the demand for light distribution. We compared our sensor with the above-listed sensors in the table below.

### *B. Photometric Stereo Algorithm*

Traditional vision-based tactile sensors always implement the photometric stereo(PS) algorithm to measure 3D geometries. As a technique for determining 3D shapes that was first proposed by Woodham [10] in 1980, PS is one of the main approaches to solving the 3D reconstruction problem of computer vision. The principle behind it is to establish the relationship between the intensity of incident light and reflected light, to determine the normal direction of each pixel on the reflected surface.

PS algorithms can be categorized based on the number of input images, and these different types of PS algorithms are widely used in vision-based tactile sensors. Lin et al. [7] used a photometric stereo algorithm with a single input image in Dtact, they utilized the disparity in light intensity reflected from the respective pixel point before and after the deformation of the gel to infer the extent of deformation at that pixel point. Although photometric stereo algorithm with two input images also exists [11], this algorithm is not used on a large scale because it does not reveal the advantages compared with algorithms with three images. On the contrary, PS algorithms with three images are used the most. There are two main reasons for this: one is that we can get three independent light maps from an image after RGB three-channel separation, and the second reason is that the constraints on the three images are just enough to make the matrix built by the algorithm full rank. Some algorithms use more than three images to reconstruct the surface, Nie et al. [12] used six images in their experiments, while S. Büyükatalay et al. [13] even used eight images. Such algorithms usually depart from the conditions of the linear equations of Lambert's Model; using more images improves the results when solving overly constrained systems and reduces the error of the pseudo-inverse solution for linear equations.

## III. LIGHT SOURCE DESIGN

In tactile sensors, the light source is vital as a light generator. Self-shadowing, cast shadows, specular areas and internal reflections are all important considerations in the light source design.

The primary purpose of the light source design is to adapt to the PS algorithm. Our light source comprises 24 phantom LEDs uniformly distributed within an 8cm diameter circle. These LEDs can emit various colors and brightness of light. Furthermore, these 24 independently controllable light sources can be flexibly combined, allowing our sensors to simulate a wide range of lighting conditions to meet the requirements of the PS algorithm.

Now, most of the VBTSs are built on the hypothesis of parallel light or use long-distance point light sources to simplify the incident light. Based on these conditions, We can significantly simplify the model and algorithm without compromising accuracy, thereby improving algorithm speed. However, it is not practical to use a remote point light source, as the long optical path would increase the size of the sensor. It seems that these constraints are difficult to be realistic for a compact sensor system, so we propose a groundbreaking approach of using multiple light sources that interact with

each other to adjust the lighting environment and achieve the optimal lighting conditions for the PS algorithm.

LED is the best choice among many light sources because of its high brightness, small size, high integration, high controllability, and other advantages. LED is a typical non-isotropic point light source and can be easily integrated and synchronized with imaging equipment. We have a higher resolution option for light control—LCD screens than LED. Bi et al. [14] attempted to utilize an LCD screen as a light source. However, they assumed that the light region of the LCD screen behaves as a point source at infinity. Due to this assumption, the authors did not provide a comprehensive model for the light equation of the LCD screen. In contrast, the LED light source has a set of mature formulas to calculate the light distribution [12], we can establish its light distribution equation by querying the LED product specification. In addition, the brightness of the LED light source is much brighter than the LCD screen.

The main reason for using phantom light source instead of the same RGB monochrome light source as GelSlim 3.0 and GelSight is to achieve uniform illumination and avoid shadows. For compact systems like VBTS, the light source are always placed very close to the imaging layer, and to ensure a large enough field of view, the light source needs to be positioned outside the imaging layer. In such situation, if there is a protrusion on the imaging layer, it will result in significant errors in the imaging of the rear view due to the projection of shadows. To avoid these issues, some PS experiments typically increase the distance between the light source and the imaging layer to ensure each individual light source can illuminate the entire surface. However, this contradicts the design principles of our sensor. We plan to arrange different ratios of RGB tricolor light for each light source instead of using monochromatic light from a single direction. This way, we can achieve uniform illumination across the entire image even after channel separation. In other words, the equivalent emitting source of the monochromatic channel is slightly offset from the edge of the imaging layer, closer to the imaging center, which helps prevent shadow projection. As for 24 LEDs, we attempt to achieve the optimal solution in quantity and spatial distribution by maintaining the number of LEDs as a multiple of three.

## IV. Lens Design and Optical Simulation

The lens design aims to concentrate the LED illumination light on the imaging plane, achieve sufficient and uniform light on the imaging surface, and enrich the information in the sensing area. Since the LED light source range is 120°, part of the light cannot illuminate the silicone reflective surface and form an image. This article designs the lens's side curved surface and upper surface curved surface to concentrate light.

This article evaluates the light path-shaping effect of the lens by simulating the refraction of light by the radial cross-section of the lens, thereby optimizing the design. In this article, 24 light sources, distributed symmetrically around the axis, are used so that the light from parallel sections can achieve complete coverage. fig. 2 shows the optical path of a single light source in the radial section and the imaging effect of the whole light source in the transverse section with no lens. It can be found that the light distribution under the transverse section is ideal, and the imaging surface is covered with light. The lens's curved surface under the radial cross-section needs to be further designed to achieve sufficient light on the imaging surface.

The incident ray is emitted from point $A$, whose direction is $\mathbf{i}$, and intersects the curved surface at point $P$. The curved surface is formed by rotating an arc around the axis $\hat{\mathbf{z}}$, where The arc is on the x-z plane, and the center of the arc is point $B$.

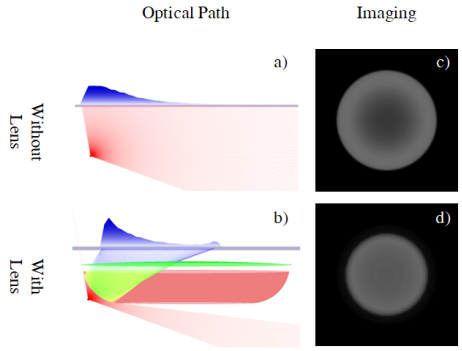


Fig. 2. Simulation result of the optical path in the radial section and imaging effect in the transverse section.

### A. Optical path simulation

To simulate the refraction effect of a curved surface on light in a plane, it is necessary to calculate the direction of the outgoing light based on the incident light and the refractive surface. The lens surface in this article is formed by rotating an arc around the z-axis. Therefore, we need to solve the intersection point and normal of the curved surface based on the incident light through geometric relationships. The algorithms for solving intersection points and normal directions in three cases will be introduced below.

*1) Case 1: Ray and arc in plane:* The particular case for light refracted on the left side of the lens.

The light source point $A$, the incident light direction $\mathbf{i}$ and the surface rotation axis $\hat{\mathbf{z}}$ are on the same plane, so the intersection problem between rays and curved surfaces in space can be simplified to the intersection problem between rays and arcs in plane. fig. 3(a) shows the geometric relationship between light and arc in this case.

Given the coordinates of points $A$ and $B$ and the direction of the incident light $\mathbf{i}$, to obtain point $P$ as the intersection point, and $\mathbf{n}$ as the normal vector, we get

$$\begin{aligned} P &= A + \overline{AP}\ \mathbf{i} \\ \mathbf{n} &= \overrightarrow{BP} \end{aligned} \tag{1}$$

where $\overline{AP}$ can be obtained by

$$\overline{AP} = \overline{AC} - \overline{CP} \tag{2}$$

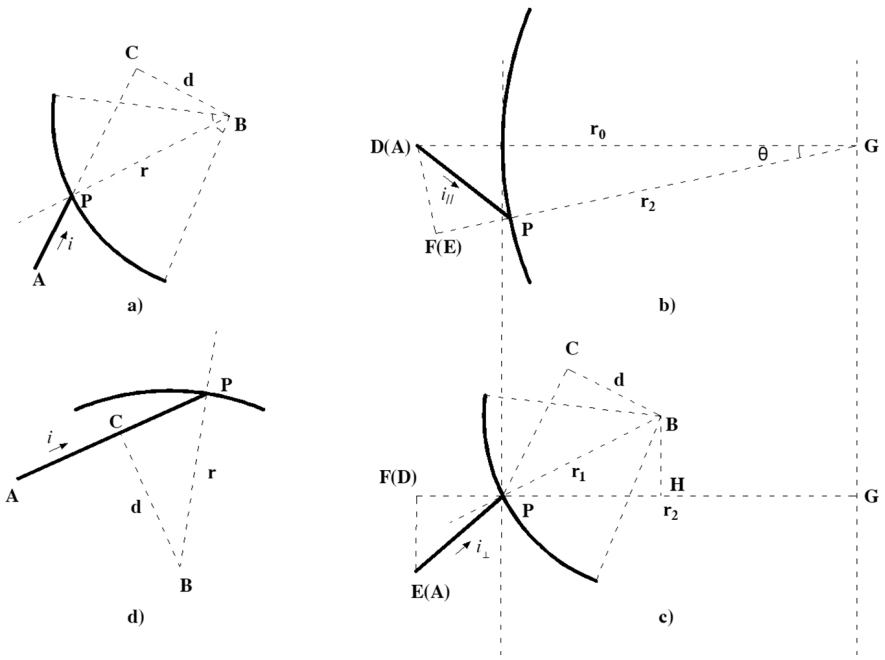


Fig. 3. Schematic diagram of intersection problems. (a) x-z plane of case 1. (b) Top view of case 2. (c) P-z plane of case 2. (d) APB plane of case 3.

From the Pythagorean theorem, we can get

$$\overline{CP} = \sqrt{r^2 - d^2} \tag{3}$$

By dot product and cross product of vectors $\mathbf{i}$ and $\overrightarrow{AB}$, we get

$$\begin{aligned} \overline{AC} &= \mathbf{i} \cdot \overrightarrow{AB} \\ d &= \left| \mathbf{i} \times \overrightarrow{AB} \right| \end{aligned} \tag{4}$$

Substitute eqs. (2) to (4) into eq. (1), and we can get the coordinates of intersection point $P$ and normal vector $\mathbf{n}$ in case 1.

*2) Case 2: Ray and curved surface in space:* The general case for light refracted on the left side of the lens.

When the light source point $A$, the incident light direction $\mathbf{i}$ and the rotation axis $\hat{\mathbf{z}}$ are in different planes, and the arc center $B$ is not on the rotation axis $\hat{\mathbf{z}}$, the intersection problem needs to be analyzed in two planes.

fig. 3(b) shows a plane passing through point $P$ and perpendicular to the z-axis. Point $D$ and point $F$ are the projections of point $A$ and point $E$ on this plane, and Point $G$ is the intersection point of the z-axis and this plane. In addition, DF is perpendicular to line GP at point F.

Given incident light direction $\mathbf{i} = \begin{bmatrix} i_1 \\ i_2 \\ i_3 \end{bmatrix}$, we can get $\mathbf{i}_{\parallel} = \begin{bmatrix} i'_1 \\ i'_2 \\ 0 \end{bmatrix}$, where $i'_1 = i_1/\sqrt{i_1^2 + i_2^2}$ and $i'_2 = i_2/\sqrt{i_1^2 + i_2^2}$.

Line $DG$ is parallel to the y-axis because Point $D$ and $G$ are on the x-z plane and perpendicular to the z-axis. Therefore, The sine and cosine of the intersection angle between line $DG$ and ray $\mathbf{i}_{\parallel}$ can be obtained by calculating cross product and dot product of vector $\mathbf{i}_{\parallel}$ and $\hat{\mathbf{y}}$.

$$\begin{aligned} \sin \angle PDG &= -i'_2 \\ \cos \angle PDG &= i'_1 \end{aligned} \tag{5}$$

For triangle $\Delta DPG$, using the sine theorem we get the following equation

$$\begin{aligned} \frac{r_2}{r_0} = \frac{\sin \angle PDG}{\sin(\pi - \theta - \angle PDG)} &= \frac{i'_2}{i'_2 \cos\theta - i'_1 \sin\theta} \\ &= \frac{i_2}{i_2 \cos\theta - i_1 \sin\theta} \end{aligned} \tag{6}$$

From eq. (6), we know the following algebraic relationship between unknowns $r2$ and $\theta$

$$r_2 = f(\theta) = \frac{i_2 r_0}{i_2 \cos\theta - i_1 \sin\theta} \tag{7}$$

fig. 3(c) shows the EPG plane, which is perpendicular to the x-y plane.

From the projection relationship, we get

$$\frac{\overline{EF}}{\overline{FP}} = \frac{\mathbf{i} \cdot \hat{\mathbf{z}}}{\mathbf{i} \cdot \overrightarrow{PG}/r2} = \frac{i_3}{i_1 \cos\theta + i_2 \sin\theta} \tag{8}$$

According to the geometric relationship in fig. 3(b), we can get the expression of $\overline{FP}$ with respect to $r_2$ and $\theta$

$$\overline{FP} = r_0 \cos\theta - r_2 \tag{9}$$

Through the eqs. (8) and (9), we can get

$$\overline{EF} = g_1(r_2, \theta) = \frac{i_3(r_0 \cos\theta - r_2)}{i_1 \cos\theta + i_2 \sin\theta} \tag{10}$$

According to the geometric relationship in fig. 3(c), we get

$$\overline{BH} = g_2(r_2) = \sqrt{r_1^2 - \left(r_2 - \overline{GH}\right)^2} \tag{11}$$

where $r_1$ is the radius of arc $B$, $\overline{GH}$ is the distance between arc center $B$ and rotation axis $\hat{\mathbf{z}}$.

Considering that $d = \overline{BH} + \overline{EF}$ is the distance between the LED light source and the plane obtained by rotating the arc center, which is a constant, according to eqs. (7), (10) and (11), the function $g(\theta)$ can be established.

$$\begin{aligned} g(\theta) &= (d - g_1(r_2, \theta))^2 - g_2(r_2)^2 \\ &= (d - g_1(f(\theta), \theta))^2 - g_2(f(\theta))^2 \end{aligned} \tag{12}$$

where we use $g(\theta) = (d - \overline{EF})^2 - \overline{BH}^2$ instead of $g(\theta) = d - \overline{EF} - \overline{BH}$ to be compatible with the situation $d = \overline{EF} - \overline{BH}$.

$\theta$ can be calculated by solving the zero point of $g(\theta) = 0$ using Newton's method. This article sets the initial value to $\theta_0 = 0$ and the number of iterations to 20.

The coordinates of the intersection point $P$ and normal $n$ in case 2 can be solved by Substituting theta into

$$\begin{aligned} P &= \left[-\cos(\theta) r_2,\ -\sin(\theta) r_2,\ A_z + \overline{EF}\right] \\ n &= \overrightarrow{BP} / \overline{BP} \end{aligned} \tag{13}$$

where $A_z$ is the z-axis coordinate of $A$, and point $B$ can be obtained by rotating the original arc center on the x-z plane around the z-axis.

*3) Case 3: Ray and spherical surface in space:* The general case for light refracted on the upper side of the lens.

The curved surface is spherical when the arc center $B$ coincides with the rotation axis $\hat{\mathbf{z}}$. Therefore, only the $APB$ plane needs to be analyzed.

Similar to case 1, given the direction of incident light $\mathbf{i}$ and the coordinates of point $A$ and point $B$, $\overline{AP}$ can be solved through geometric methods according to fig. 3(d).

$$\overline{AP} = \overline{AC} + \overline{CP} = \overrightarrow{AB} \cdot \mathbf{i} + \sqrt{r^2 - \left|\overrightarrow{AB} \times \mathbf{i}\right|^2} \tag{14}$$

Substituting eq. (14) into eq. (1), we can get the coordinates of the intersection point $P$ and the normal $\mathbf{n}$ in case 3.

*4) Refraction calculation:* The method of calculating the normal direction in three cases has been introduced previously. The direction of the refracted light can be calculated using the vector form of Snell's equation [15]. The intersection point calculated previously is the starting point of the outgoing light.

### B. Imaging simulation

In this paper, the Monte Carlo method is used to simulate the light irradiation of a single light source on the imaging plane to obtain the imaging results, and then it is rotated to obtain the imaging results of multiple light sources.

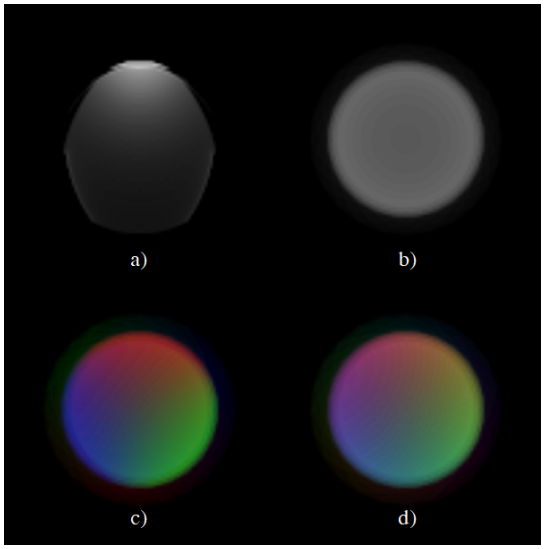


Fig. 4. Imaging simulations from different light sources emitting light of varying colors.

*1) Mono-source simulation:* For a single light source, this article simulates 1000*1000 beams of light, cast on an observation plane with a resolution of 300*300.

Light undergoes losses during the process of refraction. The Fresnel equation can be employed to calculate the intensity of the refracted light.

Considering the reflective layer as a Lambertian surface, the intensity of diffuse reflection formed by the incident light depends on the angle between the light rays and the normal vector. The light emitted by the LED point source undergoes significant directional changes upon refraction through a lens, leading to distinctive imaging effects on reflective surfaces. fig. 4(a) illustrates the imaging effects of the reflective surface under a single light source.

*2) Multi-source simulation:* The imaging results are obtained for multiple light sources by rotating and accumulating the single light source results 24 times.

For the light source $S_i$, the intensity image $I_i$ of its imaging is obtained by rotating the single-source intensity image $I_0$ around the center of the image by an angle of $\pi i/12$. fig. 4(b) illustrates the intensity image with 24 white light sources. The rotation algorithm is introduced in [16].

Different light sources emit light of various colors, thus the intensity accumulation for each pixel involves a distinct weighting scheme. For light source $S_i$, assuming its emitted light has RGB components $[c_{i1}, c_{i2}, c_{i3}]$, the RGB components $[c_1, c_2, c_3]$ of final rendering image $I$ can be obtained as

$$c_j = \mu \sum_{i=1}^{24} \sigma_i I_i c_{ij}, \quad j = 1, 2, 3 \tag{15}$$

where $\mu$ and $\sigma_i$ represent the camera's exposure time and the light source's brightness $S_i$, respectively.

fig. 4(c) and (d) respectively depict the rendering effects of multicolored light and trichromatic light. The conclusion can

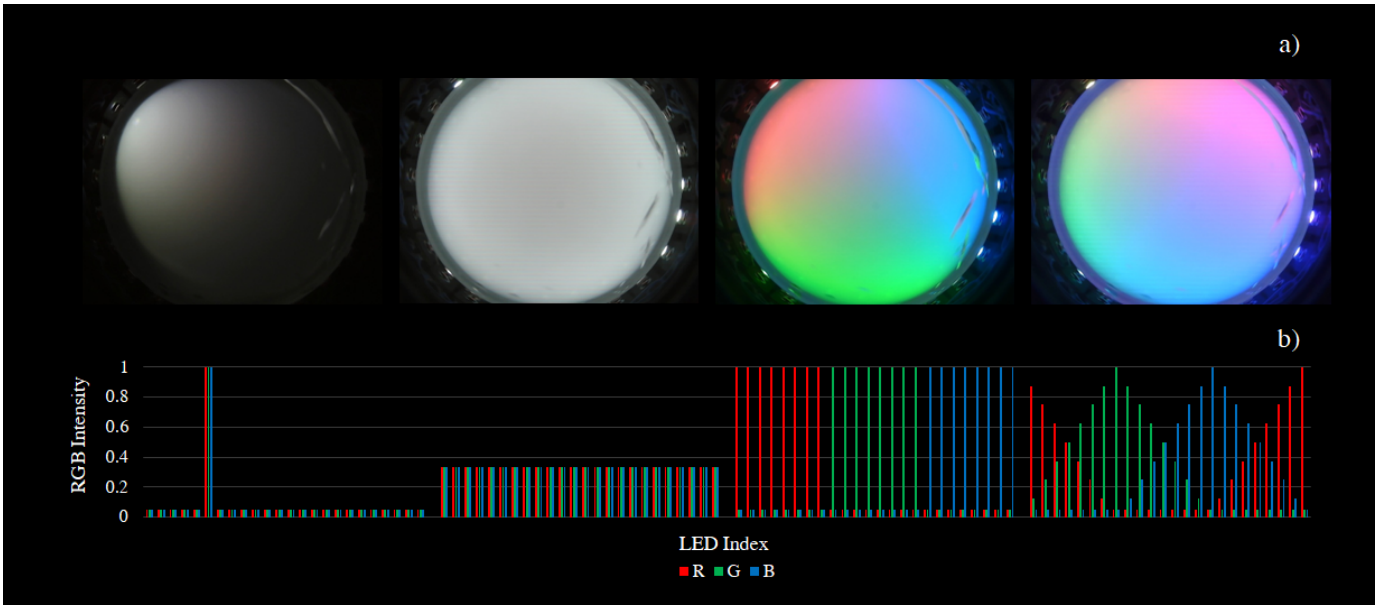


Fig. 5. Basic setup of the experiment and presentation of results (a)Actual image displayed on the IrisTac using four different lighting methods. (b)The proportional configuration of each LED in the RGB three-channel among four lighting modes

be drawn from the images that multicolored light demonstrates superior transition effects during imaging.

This chapter presents the methods for simulating optical paths and calculating imaging, upon which the lens curvature design is based. The radius of the lateral curvature is 13.5 millimeters, and the radius of the top curvature is 600 millimeters. Through simulation verification, 63.5% of the light is incident on the imaging screen without the use of the lens with an average image intensity of 5.0516. However, when the lens is employed, 78.0% of the light is incident on the imaging screen, resulting in an average image intensity of 5.326.

## V. Design Of IrsiTac and Experiments

*1) Design Of IrsiTac:* To implement our designs in a compact space, we carefully organized the arrangement of all components as shown in fig. 6.

*2) Light distribution of multicolored light:* As we mentioned in Section III, we attempt to achieve uniform illumination on the gel in each color channel by leveraging the mutual influence among multiple color lights. Rather than focusing on the overall brightness distribution of the entire image, we are more concerned about whether the brightness distribution of the three separate color images is uniformly bright after channel separation.

We try to use IrisTac to simulate the case of point light, monochromatic light, trichromatic, and multicolor light; the ratios of each LED in the three RGB channels are shown in the fig. 5.

## VI. Conclusion

We introduce a novel tactile sensor design called IrisTac, which incorporates a new light source and optical lens to update the design of the tactile sensor at an optical optimization level. Rather than describing IrisTac as a specific sensor, it is more accurate to portray it as a tactile experimentation platform. With IrisTac, researchers can simulate lighting conditions under various circumstances to assist them in conducting experiments related to tactile sensors. In contrast to neglecting multi-color light sources in other works, we discard the traditional RGB tricolor light, fully leveraging phantom LEDs' controllable brightness and color properties. We evaluate the impact of different combinations of color light on sensor performance and validate our assumptions. Throughout this process, we compare IrisTac's optical design with several similar tactile sensors, discussing their advantages

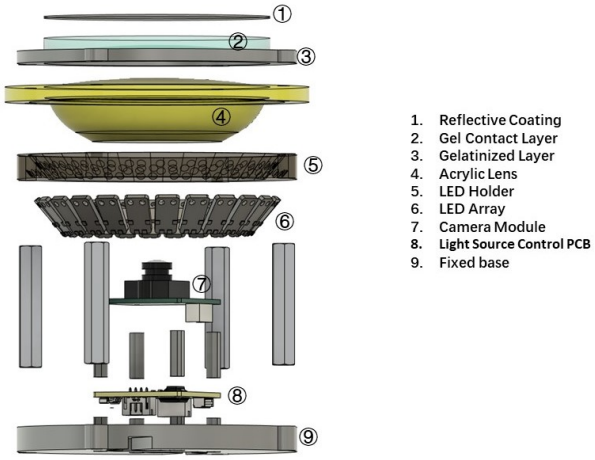


Fig. 6. Assembly diagram of the IrisTac

and limitations. Additionally, we design a simulator for light path simulation, which assists researchers in rapidly iterating through lens designs. In the future, we plan to utilize IrisTac with more suitable photometric stereo algorithms to conduct experiments such as object surface depth reconstruction and estimation of contact force distribution to showcase its superiority.

## ACKNOWLEDGMENTS

This work was supported in part by the Guangdong Natural Science Fund-General Programme under grant no. 2021A1515012384. It was also supported by the Science, Technology, and Innovation Commission of Shenzhen Municipality under grant no. ZDSYS20200811143601004, and the National Science Foundation of China(NSFC)#U1913603.

## REFERENCES

[1] I. H. Taylor, S. Dong, and A. Rodriguez, "Gelslim 3.0: High-resolution measurement of shape, force and slip in a compact tactile-sensing finger," in *2022 International Conference on Robotics and Automation (ICRA)*. IEEE, 2022, pp. 10 781–10 787.

[2] S. Wang, Y. She, B. Romero, and E. Adelson, "Gelsight wedge: Measuring high-resolution 3d contact geometry with a compact robot finger," in *2021 IEEE International Conference on Robotics and Automation (ICRA)*. IEEE, 2021, pp. 6468–6475.

[3] S. Dong, W. Yuan, and E. H. Adelson, "Improved gelsight tactile sensor for measuring geometry and slip," in *2017 IEEE/RSJ International Conference on Intelligent Robots and Systems (IROS)*. IEEE, 2017, pp. 137–144.

[4] E. Donlon, S. Dong, M. Liu, J. Li, E. Adelson, and A. Rodriguez, "Gelslim: A high-resolution, compact, robust, and calibrated tactile-sensing finger," in *2018 IEEE/RSJ International Conference on Intelligent Robots and Systems (IROS)*. IEEE, 2018, pp. 1927–1934.

[5] M. Lambeta, P.-W. Chou, S. Tian, B. Yang, B. Maloon, V. R. Most, D. Stroud, R. Santos, A. Byagowi, G. Kammerer *et al.*, "Digit: A novel design for a low-cost compact high-resolution tactile sensor with application to in-hand manipulation," *IEEE Robotics and Automation Letters*, vol. 5, no. 3, pp. 3838–3845, 2020.

[6] F. R. Hogan, M. Jenkin, S. Rezaei-Shoshtari, Y. Girdhar, D. Meger, and G. Dudek, "Seeing through your skin: Recognizing objects with a novel visuotactile sensor," in *Proceedings of the IEEE/CVF Winter Conference on Applications of Computer Vision*, 2021, pp. 1218–1227.

[7] C. Lin, Z. Lin, S. Wang, and H. Xu, "Dtact: A vision-based tactile sensor that measures high-resolution 3d geometry directly from darkness," in *2023 IEEE International Conference on Robotics and Automation (ICRA)*. IEEE, 2023, pp. 10 359–10 366.

[8] H. Jiang, Y. Yan, X. Zhu, and C. Zhang, "A 3-d surface reconstruction with shadow processing for optical tactile sensors," *Sensors*, vol. 18, no. 9, p. 2785, 2018.

[9] L. Zhang, Y. Wang, and Y. Jiang, "Tac3d: A novel vision-based tactile sensor for measuring forces distribution and estimating friction coefficient distribution," *arXiv preprint arXiv:2202.06211*, 2022.

[10] R. J. Woodham, "Photometric method for determining surface orientation from multiple images," *Optical engineering*, vol. 19, no. 1, pp. 139–144, 1980.

[11] H. Liang, L. Qi, S. Wang, S. Sun, and J. Dong, "Photometric stereo with only two images: A generative approach," in *2019 IEEE 2nd International Conference on Information Communication and Signal Processing (ICICSP)*. IEEE, 2019, pp. 363–368.

[12] Y. Nie and Z. Song, "A novel photometric stereo method with non-isotropic point light sources," in *2016 23rd International Conference on Pattern Recognition (ICPR)*. IEEE, 2016, pp. 1737–1742.

[13] S. Büyükatalay, Ö. Birgül, and U. Halici, "Surface reconstruction from multiple images filtering non-lambert regions," in *2009 16th IEEE International Conference on Image Processing (ICIP)*. IEEE, 2009, pp. 533–536.

[14] L. Bi, Z. Song, and L. Xie, "A novel lcd based photometric stereo method," in *2014 4th IEEE International Conference on Information Science and Technology*. IEEE, 2014, pp. 611–614.

[15] A. Glassner, *An Introduction to Ray Tracing*, ser. Morgan Kaufmann Series in Computer Graphics and Geometric Modeling. Elsevier Science, 1989. [Online]. Available: https://books.google.com.hk/books?id=YPblYyLqBM4C

[16] R. C. Gonzalez and R. E. Woods, *Digital image processing*. Upper Saddle River, N.J.: Prentice Hall, 2008. [Online]. Available: http://www.amazon.com/Digital-Image-Processing-3rd-Edition/dp/013168728X